RSC Advances

PAPER

View Article Online
View Journal | View Issue

Cite this: *RSC Adv.*, 2024, **14**, 38872

Ferrite-doped rare-earth nanoparticles for enhanced β-phase formation in electroactive PVDF nanocomposites

Chaymae Bahloul,[a] Siham Ez-Zahraoui,[a] Adil Eddiai,[b] Omar Cherkaoui,[c] M'hammed Mazraoui,[b] Fatima-Zahra Semlali *[a] and Mounir El Achaby *[a]

This study offers a novel method for improving the piezoelectric characteristics of polyvinylidene fluoride (PVDF) by adding lanthanated $CoFe_2O_4$ nanoparticles (CLFO), thereby addressing the critical need for effective renewable energy solutions. The novelty of this work lies in the synthesis of CLFO nanoparticles and their integration into the PVDF matrix, with polyvinylpyrrolidone (PVP) employed to ensure uniform dispersion. This was accomplished by a special co-precipitation and heat treatment procedure. Nanocomposite films were created using solvent casting with a range of CLFO concentrations (1, 3, 5, and 7 wt%). The structural, morphological, mechanical, and thermal properties of these films were all thoroughly assessed. A remarkable improvement over conventional techniques was found using X-ray diffraction and Fourier transform infrared spectroscopy, which showed up to 80% β-phase development with 3 wt% CLFO. While thermogravimetric studies showed enhanced thermal stability, scanning electron microscopy verified homogeneous nanoparticle dispersion. Mechanical tests revealed ideal stiffness, strength, and ductility at 3 wt% CLFO. Significant advances in electronics and energy harvesting are anticipated from this novel combination of PVDF's piezoelectric properties and CLFO reinforcement. By minimally influencing the environment, these advancements not only tackle the world's energy problems but also present prospective uses for renewable energy technologies.

Received 27th August 2024
Accepted 17th November 2024

DOI: 10.1039/d4ra06192f

rsc.li/rsc-advances

1. Introduction

In the last few years, energy scarcity has become a growing problem. The excessive use of fossil fuel-based non-sustainable energy supplies, like natural gas, coal, and petroleum, is the main driver of pollution and global warming, among other environmental issues.[1] Moreover, overexploitation of these energy sources makes it very difficult to provide sufficient energy for the next generation while the population is growing rapidly.[2,3] Therefore, to meet future energy needs, the development of renewable, environmentally friendly, and affordable energy sources is becoming increasingly vital. Furthermore, low-power systems can now be developed as a result of modern electronic system integration and downsizing. Other methods of supplying energy have been developed as a result of this.[4]

Ambient energy is all around us, and using it as an energy source for electronic microsystems seems to be a realistic and feasible idea. Energy harvesting, a reliable power source for low-power electronic devices, is a simplified technique that efficiently converts lost energy into useable electricity. The past few years have witnessed an important rise in the popularity and acceptance of this strategy.[2,5] In addition to extensive energy harvesting using environmental resources such as solar energy, heat, and wind, mechanical vibration-based energy harvesters have been developed. These energy harvesters have greater potential, a longer lifespan, and a relatively high power density. There are a number of techniques, including the electromagnetic, electrostatic, and piezoelectric effects, for converting mechanical vibrations into electrical energy.[6,7]

Due to their simple configuration, piezoelectric energy harvesting (PEH) systems have gained more attention. One of the important discoveries of the 19th century would include the piezoelectric phenomenon.[8] Kawai (1969) found that substantial piezoelectric effects were observed in some polymers, specifically polyvinylidene difluoride (PVDF).[9] Since then, piezoelectric polymers have drawn a lot of interest from the scientific community due to their extensive prospective uses in situations requiring the use of specially adapted microdevices.[10] PVDF and its copolymer P(VDF-TrFE) represent examples of polymers with exceptional piezoelectric properties. According to

[a]*Materials Science, Energy and Nanoengineering Department (MSN), Mohammed VI Polytechnic University (UM6P), Lot 660 – Hay Moulay Rachid, 43150 Ben Guerir, Morocco. E-mail: mounir.elachaby@um6p.ma; fatimazahra.semlali@um6p.ma; Fax: +212662010620; +212661100919; Tel: +212662010620; +212661100919*

[b]*Laboratory of Physics of Condensed Matter (LPMC), Faculty of Sciences Ben M'Sik, Hassan II University, Casablanca, Morocco*

[c]*REMTEX Laboratory, Higher School of Textile and Clothing Industries (ESITH), Casablanca, Morocco*

published research, polymers often have good flexibility, light weight, adaptability, and low acoustic impedance.[11–13] And these features make polymers attractive choices for smart electronics.[14,15] PVDF has a simple chemical structure with the main unit of (–CF_2–CH_2–) type. PVDF has five main crystalline phases, namely, phase I (α), phase II (β), phase III (γ), phase IV (ε), and phase V (ξ), with the first two structures being common. The mechanical, electrical, and thermal processing parameters utilized in producing the PVDF film determine how much of each phase is present in relation to the other. The non-polar α-phase, which lacks piezoelectric characteristics, is the most prevalent form. All of the polymer's pyroelectric and piezoelectric characteristics are attributed to the strongly orientated β-phase alone.[9] PVDF has been extensively researched because of its strong mechanical strength, unique thermal stability, and chemical resistance. This has an impact on the creation of electronic devices since PVDF is more flexible and has superior electrical properties compared to conventional materials.[16]

The piezoelectrically active β-phase possessing the highest piezoelectric, ferroelectric, and pyroelectric coefficients along with a great dielectric constant is the most technologically interesting one and highly effective for a variety of energy harvesting applications, including sensors and wearable electronics.[17] This can be achieved through a variety of techniques: first, by uniaxial or biaxial stretching of crystallized PVDF films, a method commonly used in industry; second, by crystallization of the molten polymer at high pressure; third, by inducing crystallization from solution under certain conditions; and finally, by applying high electric fields.[14,18] In addition, some studies have shown that PVDF with piezoelectric properties can be generated by nucleating charges added to the PVDF matrix to produce nanocomposites using simple phase transitions by solvent casting.[7] Among the commonly used materials in the form of ceramic is PZT. Chang *et al.*[19] fabricated PZT nanofibers *via* electrospinning and incorporated them into a PVDF composite film as a dielectric filler. Even with a low volume fraction of 2.4% PZT nanofibres, the composite film achieved the desired dielectric constant and exhibited a piezoelectric coefficient (d_{33}) of about 87.4 pC N^{-1}. Choi *et al.*[20] examined the mechanical and electrical properties of a piezoelectric hybrid structure comprising zinc oxide (ZnO) nanowires and PVDF. The ZnO nanowires enhanced the deformation range transferred to the PVDF during mechanical stress, consequently boosting the output power of the hybrid nanogenerator. On the other hand, a larger strain was applied to the PVDF within the hybrid structure as a result of NW addition, which modified the mechanical stiffness (Young's modulus) of the hybrid structure, leading to an improvement in electrical output production. In addition, the significant results obtained through our teamwork in the field of PVDF-based nanocomposite films are noteworthy. El Achaby *et al.*[21] synthesized PVDF nanocomposite films with multiwalled carbon nanotubes coated with polyvinylpyrrolidone (PVP-coated MWCNTs). As a result, PVDF nanocomposite films with significantly improved mechanical properties and enhanced β-phase polymorphism at low MWCNT content were obtained with a PVP coating (0.1 wt%).

Lately, spinel structures have emerged as an intriguing additive to polymer matrices, captivating researchers with their remarkable ability to boost the structural, mechanical and thermal properties of polymer matrices, paving the way for advancements in different fields such as energy harvesting and energy storage and beyond. In this context, Hanan *et al.* demonstrated that the addition of Co_3O_4 nanoparticles to chitosan/polyvinyl alcohol (CS/PVA) nanocomposite films enhanced their optical, mechanical, thermal, and antibacterial properties, making them suitable for optoelectronics and biological applications.[22] In addition, Elamin *et al.* discovered that the addition of Fe_3O_4 to the poly(methyl methacrylate) (PMMA)/polyaniline (PANI) composite is well-suited for electromagnetic and optical applications due to its ability to significantly enhance the structural, optical, and magnetic properties.[23] Among these spinel materials, cobalt ferrite spinel $CoFe_2O_4$ has attracted research attention because it has superior resistance to heat, high resistivity, great chemical stability, simple preparation and controllable structure.[24] Indeed, many studies have focused on the magnetic and electrical properties of PVDF when doped with $CoFe_2O_4$ nanofillers, highlighting significant enhancements.[25] However, only a few studies have delved into the structural, mechanical, and thermal effects of these additives on the overall properties of the PVDF-based nanocomposite.

In this regard, scientists have been exploring the potential for enhancing the properties of spinels by different methods. Doping ferrite nanoparticles with rare-earth elements presents a novel approach to significantly enhancing the functional properties of spinel ferrites. The substitution of Fe^{3+} ions with rare-earth ions, even in small amounts, induces structural changes and strain within the spinel lattice, leading to substantial improvements in the material's magnetic and electrical properties.[26] While the potential of rare-earth-doped ferrites has been explored, incorporating them into a PVDF matrix for the first time offers a unique opportunity to develop a multifunctional nanocomposite.[27,28] The modified ferrite particles effectively promote the nucleation of the β-phase in PVDF. Incorporating ferrite particles as fillers into the PVDF matrix not only facilitates β-phase formation but also increases the dielectric value due to significant interfacial polarization and the enhancement of electric dipoles. The nucleation of the electroactive β-phase and the resulting high dielectric properties of PVDF create a material with great potential for mechanical energy harvesting through the piezoelectric effect, as well as for electrical energy storage. As a result, the nanocomposite exhibits enhanced dielectric, ferroelectric, and magnetoelectric properties,[29,30] making it well-suited for a variety of advanced applications, such as energy harvesting, sensors, and flexible electronics.[31]

This work has been developed with a novel approach involving for the first time the synthesis of a lanthanum-doped ferrite incorporated into PVDF to enhance the electroactive β-phase. However, despite the high nucleation capability for the β-phase, this type of nanocomposite still suffers from inhomogeneity and agglomeration, as the nanoparticles tend to cluster together due to their well-known magnetic properties.

To address this, a novel approach is employed in this work: polyvinylpyrrolidone (PVP) is used as a surface modifier to achieve better dispersion of the nanoparticles and improve their interaction within the PVDF matrix. This dual approach aims to enhance the β-phase content through improved interactions: first between PVDF and PVP, and then between the nanoparticles and PVDF. This strategy addresses the current gaps in the literature concerning the use of rare-earth-doped spinel ferrites in polymer nanocomposites for energy harvesting and aims to optimize both mechanical and piezoelectric properties.

2. Materials and experimental details

2.1. Materials

Dimethylformamide (DMF, >99.8%) was used as the solvent and purchased from Alfa Aesar. The chemicals utilized in this study were obtained from Sigma-Aldrich, including polyvinylidene fluoride (PVDF) in powder form, which melts at 177 °C and has a density of 1.78 cm^3, and polyvinylpyrrolidone (PVP), which has a melting point of 150 °C and a density of 1.2 g cm^{-3}. Cobalt nitrate ($Co(NO_3)_2 \cdot 6H_2O$), lanthanum nitrate ($La(NO_3)_3 \cdot 6H_2O$) and iron chloride ($FeCl_3 \cdot 6H_2O$) were sourced from Sigma-Aldrich as well. They were all used without any further modification.

2.2. Synthesis of cobalt ferrite doped with lanthanum (La)

CLFO nanoparticles were prepared by a coprecipitation method using analytical grade cobalt nitrate ($Co(NO_3)_2 \cdot 6H_2O$), lanthanum nitrate ($La(NO_3)_3 \cdot 6H_2O$), iron chloride ($FeCl_3 \cdot 6H_2O$) and sodium hydroxide (NaOH). To obtain a 0.4 M solution, each metal salt was separately dissolved in deionized water according to its stoichiometric ratio. An NaOH aqueous solution was introduced to the mixture at once to reach pH 13 under magnetic stirring, resulting in a change in color to brown (precipitate). The mixture was then heated for one hour at 70 °C with continuous magnetic stirring. Following this step, the formed precipitate was rinsed with deionized water to remove nitrates, and dried in an electric oven at 100 °C overnight. The resulting solid was ground using a mortar. Afterward, these nanoparticles were subjected to a 3 hour calcination process at 600 °C under an oxygen atmosphere (see Fig. 1).

2.3. Preparation of nanocomposite films

PVDF-based nanocomposite films were prepared through a solvent casting route. The prepared (CLFO) nanoparticles were fully dispersed in dimethyl formamide (DMF) by ultrasonic stirring in a beaker for one hour. Polyvinylpyrrolidone (PVP) was uniformly introduced into the suspension at a consistent ratio of 10% to facilitate surface modification of the nanoparticles. This was achieved by subjecting the mixture to ultrasonic stirring in a beaker for a duration of two hours. Next, the polyvinylidene fluoride (PVDF) powder was dissolved in the appropriate proportion in DMF with continuous stirring for 3 hours. The PVDF solution and surface-modified nanoparticle suspension were thoroughly mixed after prolonged ultrasonic agitation, and homogeneous suspensions of *X*CLFO/PVP/PVDF with 1 wt%, 3 wt%, 5 wt% and 7 wt% CLFO nanoparticles were obtained. *X*CLFO/PVP/PVDF suspensions as well as pure PVDF and PVDF/PVP solutions were deposited on a glass substrate to obtain films. The films thus prepared were dried at 120 °C for 2 hours to evaporate the solvent, and then removed from the substrate. The pure PVDF and PVDF/PVP films prepared were labelled "PVDF" and "PVDF/PVP", respectively, while the PVDF based nanocomposite films were labelled "*X*CLFO/PVP/PVDF". *X* indicates the loading amount of CLFO in the nanocomposite films ($X = 1$, 3, 5 and 7 wt%) (Fig. 1).

3. Characterization techniques

3.1. X-ray diffraction

X-ray diffraction (XRD) analysis was carried out utilizing a Bruker D8 Discover with Cu Kα radiation ($\lambda = 1.54184$ nm) over a 2θ range of 10° to 70° for the examination of nanoparticles and in the range of 15–25° for the developed nanocomposite films while maintaining a 40 kV voltage and 100 mA current.

3.2. Fourier transform infrared spectroscopy

FTIR spectra of the nanoparticle powder along with neat PVDF, PVDF/PVP and *X*CLFO/PVP/PVDF films were recorded using a PerkinElmer Spectrum 2000 equipped with an ATR accessory for the films and a KBR accessory for the powder. Each spectrum was acquired in the range of 400–4000 cm^{-1} for nanocomposites, and in 600–4000 cm^{-1} for the nanoparticle powder. The samples were analyzed with an accumulation of 16 scans and a resolution of 4 cm^{-1}.

3.3. Raman spectroscopy

Raman scattering spectroscopy was performed to investigate the vibrations of the prepared nanoparticles using a HORIBA LABRAM-HR Evolution instrument under green laser irradiation in the wavenumber range 150–1000 cm^{-1}.

3.4. Scanning electron microscopy

To describe the morphology of nanoparticles and evaluate their dispersion in the polymeric matrix of films, a Zeiss EVO 10 scanning electron microscope (Carl Zeiss Microscopy, GmbH, Jena, Germany) was used. The films were cryofractured under liquid nitrogen to acquire a clean and precise fracture surface. Prior to scanning, the samples were coated with a thin layer of gold to improve their conductivity.

3.5. Thermogravimetric analysis

Thermal stability and degradation behaviors of all PVDF, PVDF/PVP and nanocomposite *X*CLFO/PVP/PVDF films were studied by thermographic analysis using a Discovery TGA (TA Instruments). The samples were heated between 25 and 700 °C at a rate of 10 °C min^{-1} in the presence of nitrogen with a gas flow of 20 ml to avoid oxidation effects.

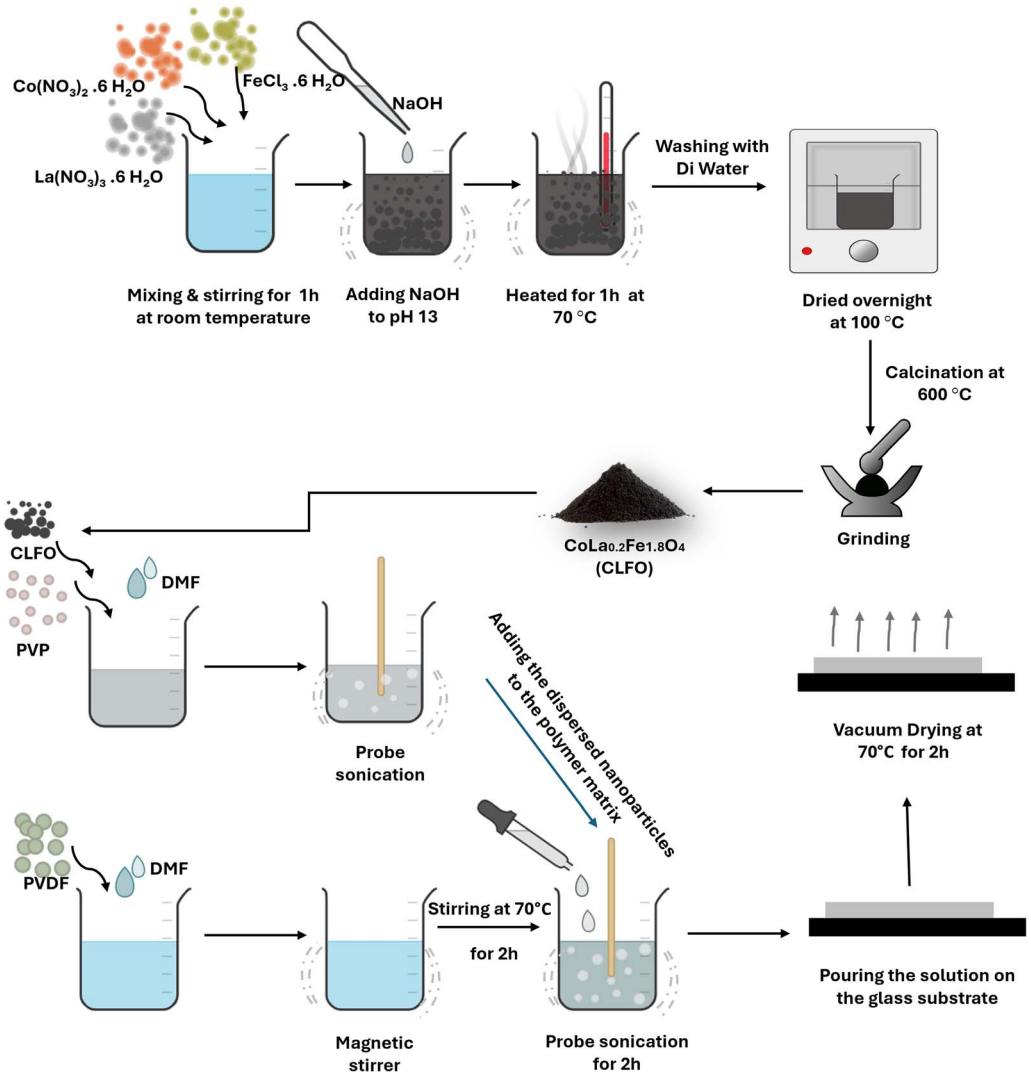

Fig. 1 Schematic of the synthesis protocol of the CLFO nanoparticles and the protocol of preparation of PVDF nanocomposite films based CLFO nanoparticles.

3.6. Differential scanning calorimetry

The behavior of elaborated films during melting and crystallization was examined with Differential Scanning Calorimetry (DSC) using a TA Instruments Discovery DSC. During the analysis process, the samples were gradually heated from 20 to 200 °C at a rate of 10 °C min^{-1}. Then, they were held at 200 °C for three minutes to eliminate any preceding thermal or mechanical effects. To better observe the samples' crystallization behavior, they were then cooled from 200 °C to −80 °C, likewise at a rate of 10 °C min^{-1}. After a stabilization period of three minutes at −80 °C, the samples were heated back from −80 to 200 °C at a similar rate as before to examine their melting properties.

The degree of crystallinity (X_c) was calculated according to the following equation:

$$X_c(\%) = \frac{\Delta H_m}{F \times \Delta H_{m_0}} \times 100 \quad (1)$$

Here, F represents the weight fraction of PVDF, and the melting enthalpy of fully crystalline PVDF (ΔH_m) is set at 104 J g^{-1}.[32]

3.7. Tensile test

The tensile properties of elaborated films were evaluated according to the ASTM D882-00 standard with a universal testing machine (SHIMADZU, Kyoto, Japan) equipped with a 1 kN load cell. The film samples were split into 10 × 80 mm^2 rectangles, with a gauge length of 50 mm and a moving clamp speed of 5 mm min^{-1}. Each test was conducted on at least five samples, and the average results were reported.

4. Results and discussion

4.1. Structural characteristics of CLFO nanoparticles

X-ray diffractogram (XRD) analysis was used as a final characterization technique to verify the crystalline phase and structure of the synthesized particles. The diffraction patterns were

examined to ensure the successful formation of the desired crystal phases and to verify the purity and structural integrity of the materials.[33]

Fig. 2 shows the XRD of the cobalt ferrite doped with lanthanum (La) rare earth element (CLFO) which illustrates eight prominent peaks attributed to the cubic spinel structure of $CoFe_2O_4$, as identified by JCPDS No. 22-1086.[34] Since (La) ion is not evidently associated with any secondary phases, it is fully integrated into the spinel lattice.[34] Using the Scherrer formula (2), the (311) plane of the spinel structures was used to calculate the size of the crystallites:[35]

$$D = \frac{0.9 \times \lambda}{\beta \times \cos\theta} \quad (2)$$

Here, D stands for the crystallite size in nanometers, λ denotes the wavelength of Co Kα radiation (1.78897 Å), β indicates the full width at half maximum (FWHM), and θ represents the diffraction angle of the most prominent peak.[36] The crystallite size remains within the range of 10.85 nm. Using the relation:

$$a = \sqrt{h^2 + k^2 + l^2} \times d_{hkl} \quad (3)$$

After calculation, the produced ferrite's lattice parameter was determined to be 8.389 Å, larger than the lattice of undoped cobalt ferrite (8.378 Å).[37] The observed increase in the lattice constant is due to the fact that the La^{3+} ions (1.06 Å), which are larger in size compared to Fe^{3+} ions (0.67 Å), replace the Fe^{3+} ions in the octahedral region. This substitution causes an expansion of the unit cell, resulting in a larger lattice constant.

Fourier transform infrared spectroscopy (FTIR) is an important complementary tool to XRD in the verification of synthesized phases. XRD provides information on the crystal structure and composition of phases, while FTIR detects the vibrations of molecules in the sample, revealing information on functional groups and chemical bonds. As shown in Fig. 3, the prepared sample was studied using Fourier transform infrared spectroscopy (FTIR) in the wavenumber range of 4000 cm^{-1} to 400 cm^{-1}. For the purpose of explaining the distribution of cations between the tetrahedral and octahedral sites of the spinel structure, FTIR spectroscopy is a precise and non-destructive technique. The FTIR spectrum shows a band at 601 cm^{-1} corresponding to the vibration of the Fe–O bonds in the crystalline lattice of the prepared nanoparticles, indicating the formation of the spinel ferrite structure. Moreover, the stretching vibration associated with the Co–O band is typically at around 866 cm^{-1}. It is unremarkable due to its low absorption and is usually obscured by the broad absorption of the Fe–O stretching vibration. It is evident from the as-prepared powder that certain organic products are present, showing comparatively weak bands that are linked to carboxylate, which is brought on by the addition of oleic acid during the nanoparticle manufacturing process. The bands at 1446 cm^{-1} and 1641 cm^{-1} are assigned to the asymmetric and symmetric $-COO^-$ stretching vibration band of the –COOH group, respectively.[38] Other specific bands of the organic oleic acid were detected at 1389 cm^{-1} and 1104 cm^{-1}, resulting from $-CH_3$ wagging deformation and the coupling of the O–H bending vibration and the C–O stretching vibration, respectively. Furthermore, the FTIR spectrum shows the characteristic bands of hydroxyl groups of water molecules adsorbed on the prepared nanoparticles at 3505 cm^{-1}, which are caused by the stretching vibration of O–H.[38]

Raman spectroscopy can be used in combination with FTIR and XRD to confirm these results and further validate the synthesized nanoparticles. It is an effective and sensitive method to detect various lattice effects that lead to changes in vibrational modes, such as lattice deformation, structural shifts, local cation distribution, charge-spin coupling, and magnetic ordering.[39] Cobalt ferrites (Fig. 4) are known to have a cubic spinel structure with an inverted space group *Fd3m*. Metal cations can occur in one of the two configurations: with four oxygen ions forming a tetrahedron or six oxygen ions forming an octahedron. This structure provides 39 normal modes, and five among them are Raman active (A_{1g} + $1E_g$ + $3T_{2g}$).[40] In this case, one-dimensional, two-dimensional, and three-dimensional representations are denoted by the initials A, E, and T, respectively. The symbol g stands for symmetry in relation to the center of inversion.[41] The five Raman modes mentioned above, which are activated in the spinel structure, are also assigned to the movement of the metal ion complex

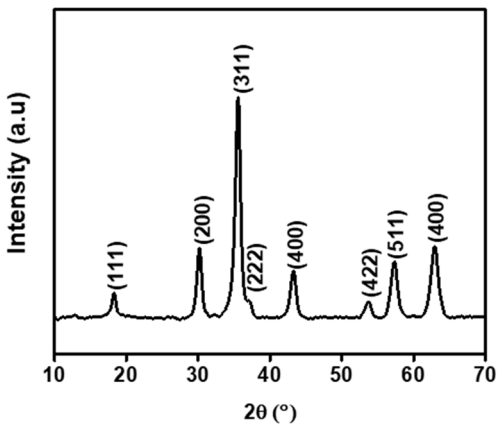

Fig. 2 X-ray diffraction (XRD) pattern of CLFO nanoparticles.

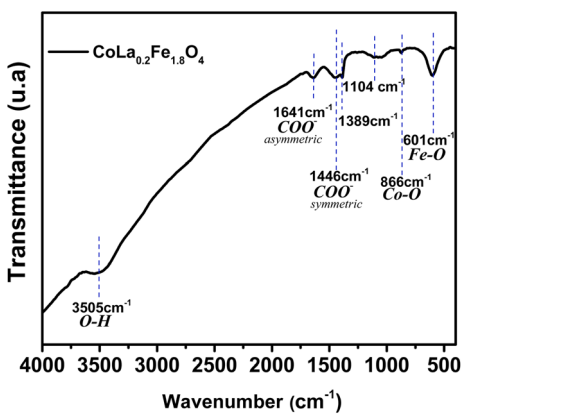

Fig. 3 FTIR spectra of the synthesized CLFO nanoparticles.

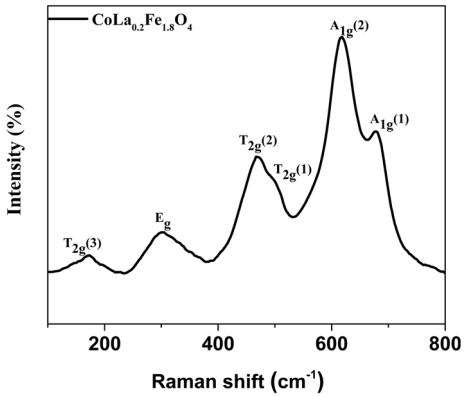

Fig. 4 Raman spectra of the synthesized CLFO nanoparticles.

O^{2-}. Therefore, between 600 and 720 cm^{-1}, tetrahedral FeO_4 exhibits a symmetric stretching known as A_{1g}, and E_g has peaks between 250 and 360 cm^{-1} due to O_2's symmetric bending with respect to Fe. In addition, T_{2g} (2) represents antisymmetric stretching of Fe and O appearing from 450 to 520 cm^{-1} and T_{2g} (1) represents the translational motion of FeO, within the range of 180 to 220 cm^{-1}. Our results and the latter assumption are largely consistent. However, previous studies have shown that the observed frequency of Raman oscillations of the prepared spinel is slightly shifted compared to undoped cobalt ferrite and this difference can be attributed to the varying masses of the cations Fe^{3+} and La^{3+} along with the disparity in their radii (La^{3+}, 1.032 Å and Fe^{3+}, 0.64 Å), which affects Fe^{3+}–O^{2-} interactions.[42]

4.2. Morphological and chemical characteristics of CLFO nanoparticles

Fig. 5(a)–(c) represent the SEM images of the CLFO nanoparticles prepared. The images were taken at a low resistance of 1 μm; even so, it was impossible to see the shape of the nanoparticles, which confirmed their nanosize. Furthermore, the SEM images depict the presence of agglomerated nanoparticles owing to their small size and the preparation method influence. Moreover, elemental composition analyses shown in Fig. 5(d) were carried out using energy dispersive X-ray spectroscopy (EDX), which confirmed the presence of Co, La, Fe and O in the sample without any additional impurities.

4.3. Structural analysis of PVDF-based CLFO nanocomposite films

For investigating the crystalline structure of pure PVDF, PVDF/PVP and *X*CLFO/PVP/PVDF nanocomposite films, XRD and FTIR characterization was used. The XRD patterns are depicted in Fig. 6(a). As shown in this figure the XRD measurements were performed from 15 to 25°. From this, the neat PVDF film

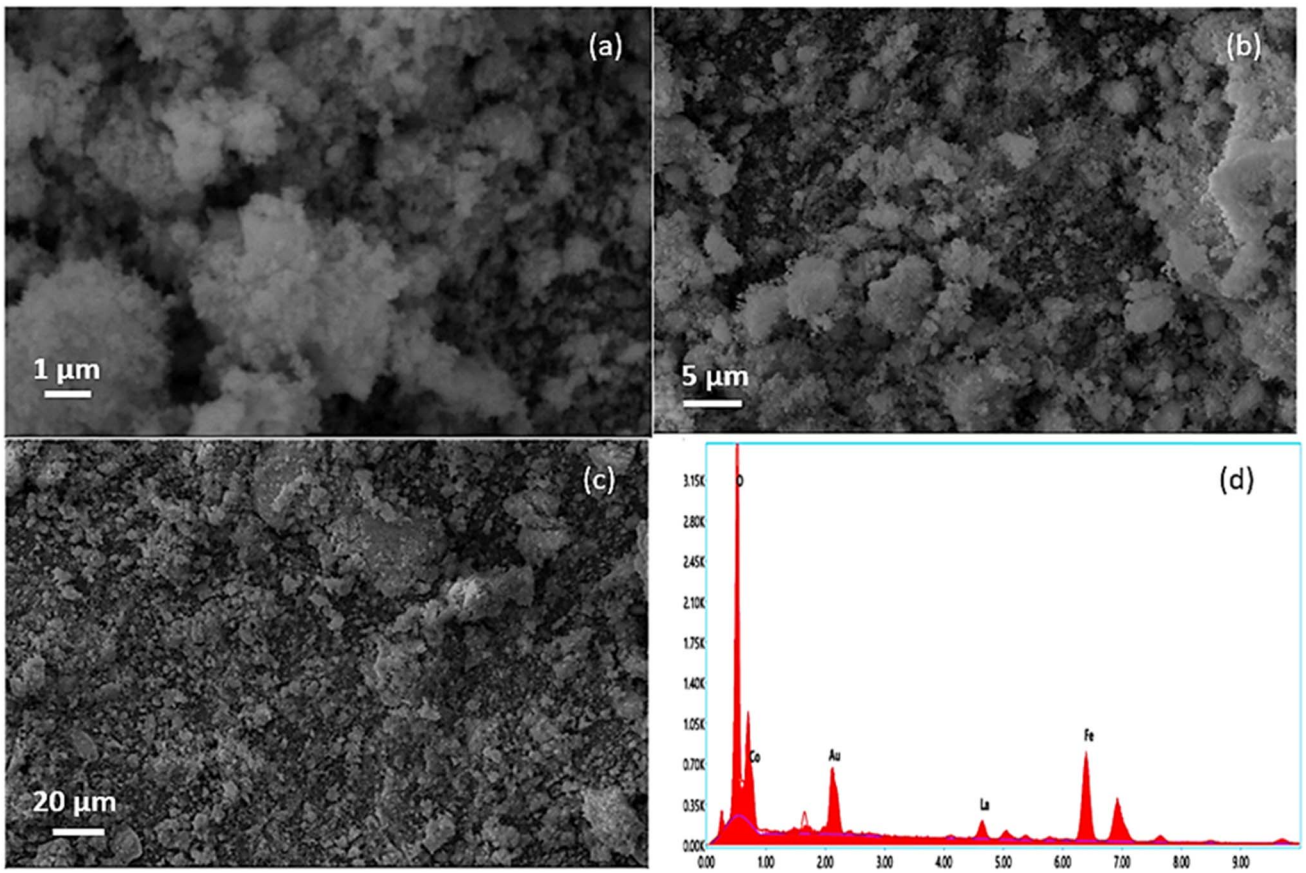

Fig. 5 (a)–(c) SEM images of CLFO nanoparticles and (d) EDX of CLFO.

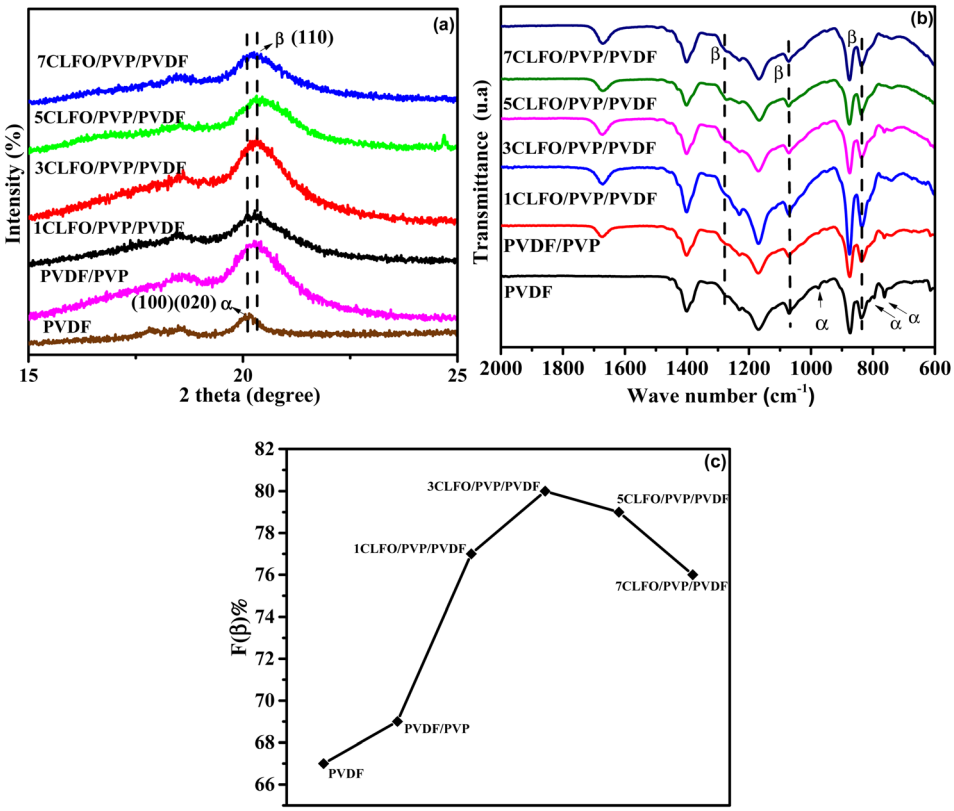

Fig. 6 (a) XRD, (b) FTIR, and (c) β-phase fraction of the films.

showcases considerable peaks at $2\theta = 17.8°$, 18.8° and 20°, which are all assigned to the non-polar α-phase crystalline structure.[21,43,44] These peaks correspond to the planes (020), (100) and (110) and *d*-spacing values of 5.00, 4.96, and 4.43 in that order. These findings suggest that the single phase present is the α-phase in a TGTG arrangement. Hence, we can draw the conclusion that PVDF's crystalline phases remain unchanged regardless of the processing conditions.[21]

The impact of blending polyvinylpyrrolidone (PVP) with the pure polyvinylidene fluoride (PVDF) matrix was explored with the goal of enhancing and stabilizing the distribution of nanoparticles within the PVDF matrix, utilizing PVP as a surface modifier. The XRD pattern of the resulting PVDF/PVP exhibits a different peak at 20.3°, which makes the multiphase semi-crystalline structure of the polymer blend clear,[45] indicating the change in the crystalline structure, which can conclude the presence of interaction in the polymer blend. Furthermore, the presence of this peak aligns perfectly with the crystalline β-phase in a TT conformation, along with an attenuated characteristic reflection attributed to the α-phase with a TGTG conformation. Importantly, the findings indicate that the addition of even a small amount of PVP can significantly modify the structure of the PVDF, causing the presence of the crystalline β-phase with a TT conformation.[45] The transformation is ascribed to the improved compatibility of PVDF and PVP, which is made possible by the creation of a hydrogen bond between the hydrogen atom of PVDF and the oxygen atom of the carbonyl group in PVP.[46]

Simultaneously, the XRD patterns of *X*CLFO/PVP/PVDF nanocomposites, featuring varying percentages of loaded nanoparticles, reveal a broad peak at 20.3°, indicating the presence of the β-phase. Corresponding to the (100) and (200) planes, this alignment perfectly matches the crystalline β-phase in a TT conformation. These observations suggest that a transition from the α to the β-phase of the PVDF crystalline structure occurs within the composite films.[47] Meanwhile, according to Mohamed *et al.*,[45] there is a relationship between peak intensities and the crystalline structure of polymers. Alharbi *et al.*[16] also noted that changes in the organization or conformation of polymer chains could lead to a decrease in crystallinity when nanoparticles are added. Comparing this to our results, we observe that varying the percentage of CLFO nanoparticles results in different XRD peak intensities. This suggests that the percentage of CLFO loading alters the structural composition of the nanocomposite. Therefore, we can conclude that the crystalline structure of the polymer matrix is significantly affected by the addition of nanoparticles. This modification is likely due to the electrostatic interactions between the nanoparticles and the polymer blend.[16,45]

This shift is attributed to potential interactions between the CLFO and PVP structures and the PVDF chain. In particular, electrostatic interactions between CLFO and PVDF promote the rotation of the C–F bonds in the PVDF chain,[46] lowering the energy barrier and encouraging the development of a more expansive *trans*-conformation, which causes the β-phase to occur. This comprehensive analysis underscores the intricate

interplay of PVP and CLFO in influencing the PVDF matrix's crystalline structure.[48]

Here, the polymorphism of pure PVDF, PVDF/PVP and *X*CLFO/PVP/PVDF nanocomposite films was investigated using FTIR (Fig. 6(b)), to further confirm the XRD findings. This is observed by the appearance of specific transmission bands in the FTIR spectra. The transmittance bands at 615 cm^{-1}, 763 cm^{-1}, 792 cm^{-1}, and 979 cm^{-1} were identified as the wagging mode of CF_2, CF_2 bending, CH_2 rocking, and twisting mode of CF_2, respectively, based on the FTIR spectra. These bands correspond to the α-phase.[49] Those bands are clearly depicted in the neat PVDF spectrum. In addition, from the FTIR spectra of the PVDF/PVP and the *X*CLFO/PVP/PVDF nanocomposites supplementary peaks are shown. A broad peak at 838 cm^{-1} which is assigned to CH_2 rocking implies the presence of the β-phase in the films. In addition, the chemical composition of the interface can be probed using Fourier transform infrared spectroscopy (FTIR) to assess whether or not chemical bonding has occurred. Indeed, if a new and different IR absorption band has been created, it may be due to the new bonds formed at the interface between the polymer and the nanoparticle surface.[50]

The absence of new bands or shifts in band positions in the FTIR spectra of the *X*CLFO/PVP/PVDF nanocomposite suggests a lack of chemical interaction between CLFO nanoparticles and other components (PVDF and PVP), indicating a predominantly physical interaction.[44,51] This finding aligns well with the explanation of the suggested physical interaction, specifically ion–dipole interactions between CLFO and PVDF.[52] Consistently, the assumption made in the preceding section holds true, indicating that the transformation from the α-phase with a TGTG conformation to the crystalline β-phase with a TT conformation for the nanocomposites is attributed to both PVP and CLFO.

This transformation is further supported by quantitative data, revealing the percentage of the β phase in various samples. The β-phase percentage in PVDF is determined through the following formula:

$$F(\beta) = \frac{A_\beta}{\left(\frac{k_\beta}{k_\alpha}\right)A_\alpha + A_\beta} \quad (4)$$

In the given formula, $F(\beta)$ represents the amount of the β-phase present, while A_α and A_β correspond to the integral areas of the bands at 763 cm^{-1} and 840 cm^{-1}, which are indicative of the α-phase and β-phase, respectively. Additionally, K_α and K_β denote the absorption coefficients at their specific wave numbers. K_α measures 6.1×10^4 cm^2 mol^{-1}, while K_β measures 7.7×10^4 cm^2 mol^{-1}.

Specifically Fig. 6(c) shows that, for the pure PVDF fraction, the β-phase constitutes 67%, while the PVP/PVDF mixture shows an increase to 70%. Notably, the addition of just 3 wt% of CLFO nanoparticles results in a maximum β-phase percentage of 80%, confirming the substantial influence of both PVP and CLFO in driving the transformation from the α to β-phase in the PVDF system.

It is important to note that creating the PVDF nanocomposite with a higher electroactive phase content requires an understanding of interfaces in the nanocomposite. It is well known that ferrite nanoparticles in general have a negatively charged surface. However, they do not proceed with the same effectiveness in nucleating the β-phase of PVDF due to the size, the morphology, and so on.[53] Without a doubt, the electric interactions between the partially positive CH_2 bonds of the PVDF and the negatively charged ferrite nanoparticles are the only explanation for the β-phase nucleation process.[54] It is shown that adding a tiny amount of CLFO nanoparticles to the PVDF/PVP blend results in PVDF films with a high electroactive β-phase content. The presence of negatively charged CLFO nanoparticles that will engage with the polymeric CH_2 groups that have a positive charge density explains the nucleation through electrical interactions. The β-phase, which has piezoelectric and ferroelectric capabilities, is formed when this contact causes the polymer chains to align on the nanoparticle surface in an extended TTTT conformation.[46] Furthermore, the possible formation of hydrogen bonding between the carbonyl group C=O of PVP and the methylene group CH_2 of PVDF can significantly contribute to the nucleation of the β-phase, which explains the increase to 70% β-phase while adding PVP to the PVDF matrix. This interaction promotes strong interfacial bonding, which facilitates the alignment and reorientation of the PVDF polymer chains. The presence of PVP enhances the compatibility between the filler and the PVDF matrix, reinforcing the stabilization of the β-phase conformation. As a result, this hydrogen bonding mechanism plays a crucial role in acting as a nucleating agent, thereby further increasing the β-phase content in the nanocomposite.

However, it is evident that above 3 wt% CLFO nanoparticles, β-phase percentage begins to decrease, reaching 76% at 7 wt%. Likewise, similar trends have been observed in various studies,[27,55,56] and these observations can be attributed to the introduction of a high concentration of nanoparticles influencing the interactions between nanoparticles and polymer chains. This phenomenon is multifaceted and involves a number of factors, including confinement effects.[57] Specifically, the confinement of the polymer chain caused by the presence of nanoparticles may limit the mobility of the polymer chain, thereby affecting favorable conditions for β-phase crystallization. Another relevant aspect is the possibility of the addition of a higher fraction of CLFO nanoparticles initiating clustering, which can interfere with the nucleation and growth of the β-phase in PVDF. As previously discussed, the nucleation of the β-phase is driven by the interaction between the negatively charged nanoparticles and the dipole moments of PVDF, which promotes interactions that facilitate β-phase formation. However, with the addition of a higher fraction of CLFO, the nanoparticles begin clustering, which disrupts this interaction. Clustering hinders the ability of the nanoparticles to effectively interact with the PVDF, thereby hindering the nucleation and growth of the β-phase.[58]

To assess the effectiveness of the proposed nanocomposite, the results achieved were compared with other newly published studies that involved the preparation of PVDF nanocomposites

Table 1 Comparison of β-phase content and dispersion quality in various PVDF based nanocomposites

Nanocomposite type	Used method	Percentage of the filler (%)	β-Phase content (%)	Comments on dispersion	Ref.
$CoFe_2O_4$/PVDF	Tape-casting route	7 wt%	49.7	Good	61
PVDF/$ZnFe_2O_4$	Electrospinning	5 wt%	83	Agglomeration	62
PVDF/Fe_2O_3	Solvent casting method	5 wt%	∼80	Some agglomeration	63
3CLFO/PVP/PVDF	Surface modification and solvent casting method	3 wt%	80	Good	This work

with a higher β-phase content. Suresh *et al.*[59] showed that cobalt ferrite ($CoFe_2O_4$) nanoparticles have an effective impact on the dielectric and ferroelectric properties of PVDF, mainly the effectiveness of the nucleation of the β-phase, where 80% of β-phase was obtained by the addition of 5 wt% $CoFe_2O_4$ to PVDF. In another study, using the same fraction of cobalt ferrite nanoparticles (5 wt%) they reached a β-phase content of 53% in the thin film.[52] In a recent study, Bhiogade *et al.*[60] reported using spin coating to create nanocomposite films with varying weight percentages of cobalt ferrite (CFO). A maximum of β-phase content of approximately 80% was noticed with 15 wt%. By comparison, by adding only 3 wt% CLFO, we were able to reach this percentage and a higher level of the electroactive β-phase. This demonstrates the efficacy of our methodology and the compositional choices. Table 1 provides an overview of the β-phase fraction, the weight percentage of nanoparticles, and the dispersion capabilities achieved using different methods. It highlights that our approach is the optimal one, achieving a high β-phase content, even at low nanoparticle concentrations (3 wt% CLFO), while ensuring excellent dispersion. This makes it an efficient and effective method compared to other routes.

To conclude, the results suggest that the nanocomposites developed successfully undergo a significant phase transition from the α to the electroactive β-phase, which is responsible for the piezoelectric properties in these materials. This discovery underlines the potential of this material for applications in energy harvesting and piezoelectric devices.

4.4. Morphological observations of PVDF-based CLFO nanocomposite films

SEM images displaying the cryofractured surfaces of the neat PVDF, PVDF/PVP blend and *X*CLFO/PVP/PVDF nanocomposite (as an example) are depicted in Fig. 7. SEM was used to investigate the interaction between CLFO nanofillers, PVDF and PVDF/PVP matrix along with the interfacial adhesion between them and better visualize the dispersion and distribution of CLFO nanoparticles in the PVDF matrix. The micrograph of unloaded PVDF and PVDF/PVP exhibits a relatively smooth surface compared with the micrograph of the 7CLFO/PVP/PVDF nanocomposite, which shows a rougher surface. It is obvious that the surface roughness dramatically rises when the concentration of the nanofiller is increased. Furthermore, no surface cracks are observed, which confirms that the nanocomposites are not weakened by the addition of nanoparticles.[64] In addition, materials with rougher surfaces require a greater force to break the polymeric phase, resulting in less brittle materials.[64]

It is worth noting that achieving a homogeneous dispersion of CLFO nanoparticles within the PVDF matrix poses significant challenges, as poor dispersion can lead to agglomeration, negatively impacting the mechanical properties and overall functionality of the nanocomposite material.[65] Likewise, high concentrations of CLFO could result in brittleness, reducing the composite's flexibility and toughness. Therefore, balancing the amount of nanoparticles is crucial to achieve the desired mechanical performance. For this raison, the polyvinylpyrrolidone (PVP) was used to coat the surface of CLFO nanoparticles to improve their dispersion.[66] Table 1 illustrates how different preparation methods influence the dispersion of ferrite nanoparticles in PVDF.

Meanwhile, the results suggest homogeneous dispersion and therefore the existence of a good affinity between CLFO nanofillers and the PVDF matrix.[44,51] In fact, even though the SEM images are at the micrometer scale, there is no evidence of any clustering of nanosized particles or of any areas where they may appear denser. This could be verified by the XRD, in which the highly dispersed nanoparticles might not form appropriately large crystalline domains to construct distinct XRD peaks. This dispersion, while being beneficial for uniformity and performance, leads to a lack of identifiable peaks for the nanoparticles. Indeed, the good affinity and the interfacial adherence may be related to the interface of the PVP modified CLFO nanoparticles which can bind strongly to PVDF, resulting in vast interface compatibility between the CLFO nanoparticles and the PVDF matrix.[44,67] This can be elucidated by the interaction between the CF_2 fluorine group of PVDF and C=O carbonyl group of PVP as supported by the FTIR result.[68]

4.5. Thermal stability of PVDF-based CLFO nanocomposite films

4.5.1. Thermal gravimetric analysis (TGA and DTG). Thermogravimetric analysis (TGA) is a fundamental analytical method widely used to reveal complex details about the thermal characteristics of polymers and polymer nanocomposites. Table 2 presents the basic data, including the degradation onset temperature (T_{onset}), the temperature of maximum degradation rate (T_{max}) obtained from the peak of the mass loss derivative, and the residue content representing the residual mass at 550 °C.

The degradation onset temperature (T_{onset}) and the temperature of maximum degradation rate (T_{max}) are critical indicators

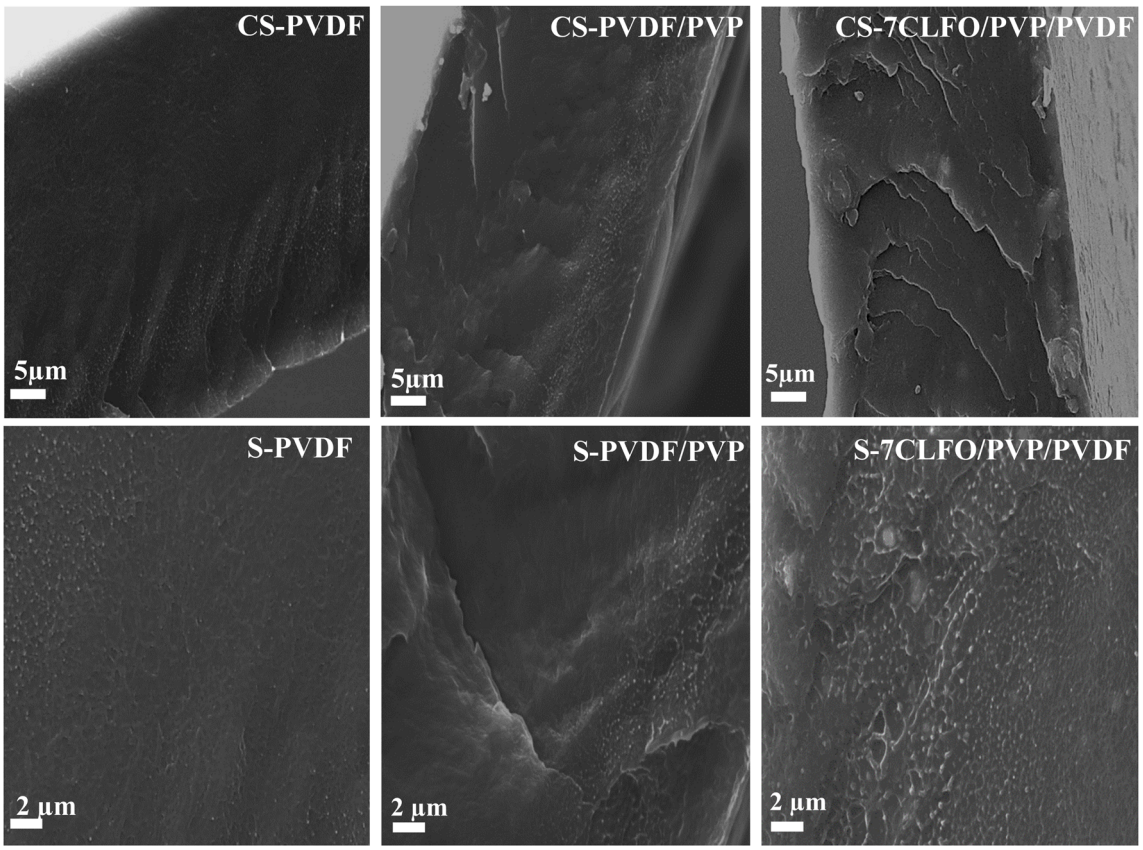

Fig. 7 SEM micrograph of the cross section (CS) and surface (S) of PVDF, PVDF/PVP and 7CLFO/PVP/PVDF films.

Table 2 Thermogravimetric results of pure PVDF and composites

Samples	T_{onset} (°C)	T_{max} (°C)	Char content (%)
PVDF	436.03	460	19.88
PVDF/PVP	341.11	454	37.61
1CLFO/PVP/PVDF	354.34	473	35.21
3CLFO/PVP/PVDF	352.15	474	35.69
5CLFO/PVP/PVDF	353.48	475	35.91
7CLFO/PVP/PVDF	358.61	477	39.06

of thermal stability. As shown in Fig. 8, for pure polyvinylidene fluoride (PVDF), the T_{onset} is 436.03 °C, and the T_{max} is 460 °C, which are consistent with known literature values,[69] indicating an elevated degree of thermal stability. When polyvinylpyrrolidone (PVP) polymer is blended with the PVDF matrix, the T_{onset} notably decreases to 341.11 °C, indicating that the introduction of PVP lowers the thermal stability of the blend. This could be related to the more amorphous nature of PVP, which can affect the overall crystallinity of the blend, leading to lower thermal stability.[70] Hossein Mahdavi *et al.*[69] achieved a similar trend. However, as CLFO nanoparticles are incorporated into the PVDF/PVP blend, the T_{onset} increases gradually with the nanoparticle content, reaching 358.61 °C at 7 wt%, which remains lower than that of pure PVDF but the nanocomposite exhibits improved stability compared to the PVDF/PVP blend without nanoparticles. Indeed, the T_{max} shows a similar trend. The T_{max} of pure PVDF is 460 °C, which somewhat decreases to 454 °C for the PVDF/PVP blend, indicating a reduced thermal stability. Upon the addition of 1% to 7% nanoparticles, T_{max} increases steadily from 473 °C to 477 °C, surpassing the T_{max} of both pure PVDF and the PVDF/PVP blend. This suggests that the nanoparticles enhance the thermal degradation resistance of the blend, likely due to the barrier effect provided by the nanohybrids, which inhibit the thermal motion and decomposition of the polymer chains.[5,71]

Comparing these results with other studies, the increase in thermal stability with nanoparticle incorporation is consistent with literature findings where various fillers, such as carbon nanotubes, clay, and metal oxides, have been reported to enhance the thermal stability of PVDF based nanocomposites. The char content also increases with nanoparticle incorporation, indicating the formation of a protective layer that further enhances the thermal resistance.[71] Overall, the incorporation of CLFO nanoparticles effectively improves the thermal stability of PVDF/PVP blends, as evidenced by the higher T_{onset} and T_{max} values compared to the PVDF/PVP blend lacking nanoparticles.

In conclusion, the present results highlight the prominent role played by CLFO in improving the thermal stability of nanocomposites. Its overall favorable contributions, acting as a reinforcing agent and having a positive impact on crystallinity, indicate a favorable effect on the material's overall mechanical properties. Consequently, these results make this developed

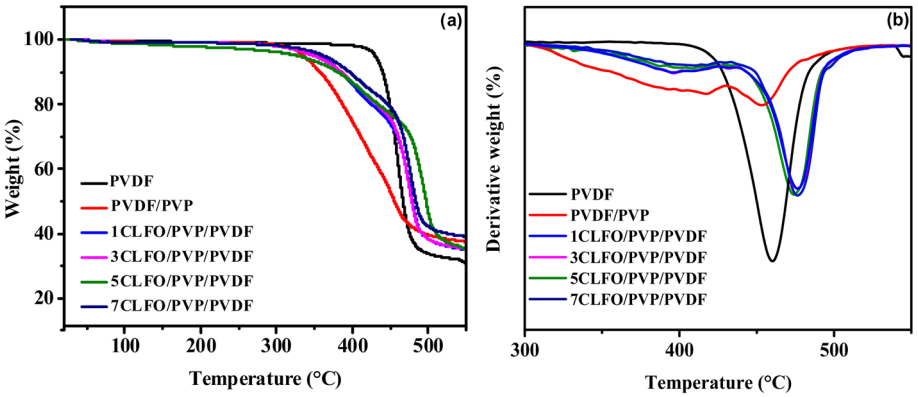

Fig. 8 TGA (a) and DTG (b) curves of PVDF-based CLFO nanocomposite films.

Table 3 Summary of DSC analysis results of the elaborated films

Samples	T_m (°C)	ΔH_m (J g^{-1})	T_c (°C)	ΔH_c (J g^{-1})	X_c (%)
PVDF	160.48	22.87	153	30.08	22
PVDF/PVP	155.72	20.38	118	34.42	21
1CLFO/PVP/PVDF	155.80	24.35	120	34.01	26
3CLFO/PVP/PVDF	154.01	24.42	118	33.95	27
5CLFO/PVP/PVDF	154.35	25.03	119	33.03	28
7CLFO/PVP/PVDF	154.31	26.01	118	32.73	30

material a convincing choice for advanced energy harvesting and piezoelectric applications.

4.5.2. Differential scanning calorimetry (DSC). To explore the phase transition behaviors of the synthesized PVDF nanocomposites, Differential Scanning Calorimetry (DSC) was utilized. Table 3 details the melting temperature (T_m), enthalpy of melting (ΔH_m), crystallization temperature (T_c), enthalpy of crystallization (ΔH_c) and degree of crystallinity (X_c).

As shown in Fig. 9(a), the semi-crystalline neat PVDF exhibits a melting temperature (T_m) of around 160 °C. It was noticed that the melting point somewhat decreased to around 156 °C when PVP was added. This can be attributed to the fact that when an additional polymer, which exhibits miscibility with the amorphous regions of the semi-crystalline polymers, is introduced, it leads to a reduction in the melting point of the crystalline polymer.[72] Even though the amount of reduction in the present case appears to be small simply because a small amount of PVP was used, the melting temperatures for all the composites with different percentages remain relatively unchanged, stabilizing around 154 °C. This may be attributed to the nanofillers having minimal impact on the molecular structure of the PVDF/PVP. This supports an earlier FTIR finding that suggested that the interaction between the polymer and nanoparticles was likely physical in nature.[73]

The crystallization temperature (T_c) of the neat PVDF is around 153 °C as depicted in Fig. 9(b), it shows a significant decrease to 118 °C when adding PVP and it remains constant when adding different percentages of the CLFO nanoparticles. The crystallization enthalpy (ΔH_c) exhibits a distinct behavior upon the addition of PVP to the PVDF in comparison to the addition of varying percentages of CLFO nanoparticles. As shown in the results in Table 3, the enthalpy of crystallization of PVDF/PVP is nearly 4 °C higher than the ΔH_c of neat PVDF. It remains unchanged when only 1 wt% CLFO is added. However, the difference becomes slightly significant when a higher percentage of CLFO is added. The marked drop in crystallization temperature and enthalpy can be explained by two factors. Firstly, the rising molecular weight of PVP leads to higher melt

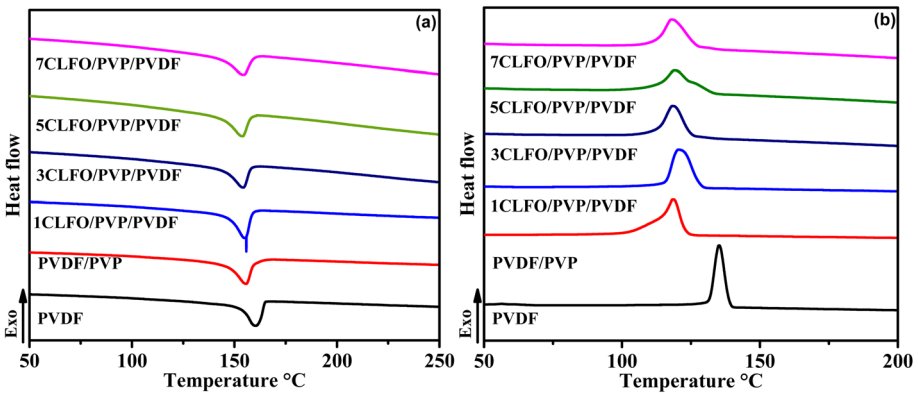

Fig. 9 Melting (a) and crystallization (b) thermograms of PVDF-based CLFO nanocomposite films.

viscosities in the blends. Indeed, higher viscosity means that the material flows less easily when heated. This can hinder the movement of polymer chains, which is essential for crystallization.[74] Secondly, the extended PVP chains create stronger entanglement with PVDF, thereby suppressing its crystallization behavior.[74] However, the ΔH_c also supports how the nanoparticles could influence the crystallization behavior. The decrease of the latter could be influenced by the nature of the interaction happening between the nanoparticles and the polymer blend.[72] Furthermore, a rise in the percentage of crystallinity is noticed upon the inclusion of nanoparticles. The reason for this enhancement is that the nanoparticles act as heterogeneous nucleating agents, promoting PVDF crystallization.[44,72]

In summary, as the crystallinity is intrinsically linked to the unique characteristics of the material, the development of higher crystalline films using the synthesized nanoparticles could positively influence the specific properties of the films, such as mechanical performance.

4.6. Tensile analysis of PVDF-based CLFO nanocomposite films

Generally, a material's mechanical properties are crucial since they determine its suitability for various applications.[51,75,76] For nanocomposites to show significant improvements in mechanical properties, it is crucial to guarantee that the nanoparticles are uniformly distributed throughout the matrix and possess robust intrinsic mechanical characteristics.[21] Additionally, it is important to consider how well the polymer chains and nanofillers interact.[21] To thoroughly investigate the mechanical behavior of the prepared nanocomposite films, tensile tests were conducted, as shown in Fig. 10.

The parameters obtained from the tensile stress–strain graph include Young's modulus, tensile strength, and strain at break. Young's modulus measures how much mechanical energy a composite material can store during reversible elastic deformation. Several factors influence tensile strength, including particle size, shape, dispersion and distribution in the polymer matrix, and their interfacial interaction. Strain at break, which is the deformation at break, provides insight into the ductility and flexibility of the films. Higher strain at break values indicate greater flexibility.[77–79]

The findings show that Young's modulus, tensile strength, and strain at break (Fig. 10(a) and (b)) significantly increased with the addition of CLFO nanoparticles across all nanocomposite samples (1, 3, 5, and 7 wt%) compared to neat PVDF. With just 3 wt% CLFO, Young's modulus reached a maximum increase of 25%, attributed to the reinforcing effect of the rigid CLFO nanoparticles, enhancing the stiffness of the nanocomposite films. Beyond 3 wt% CLFO, Young's modulus decreases, likely due to nanoparticle agglomeration disrupting uniform stress distribution and reducing reinforcing efficiency.[80]

Similarly, the tensile strength shows a moderate increment and remains generally consistent with a maximum increase of 10% observed for the nanocomposite with 3 wt% content of

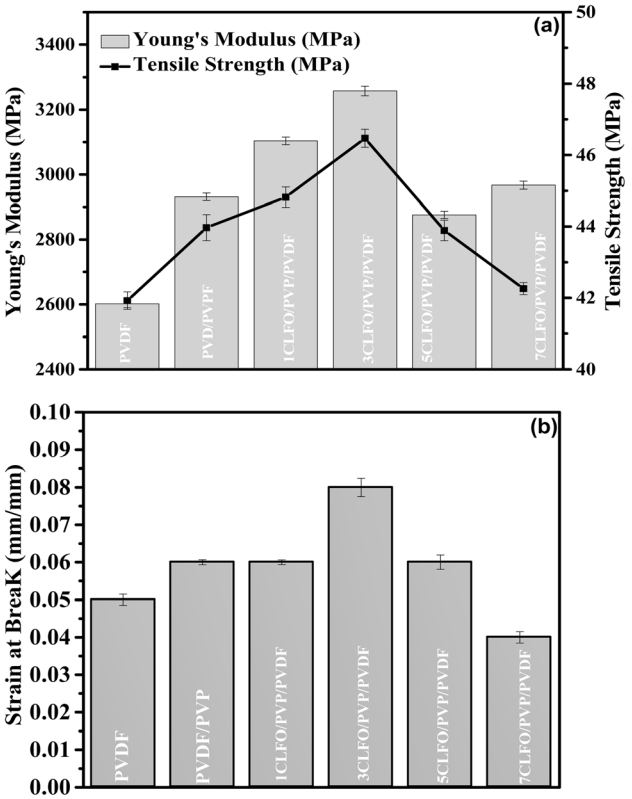

Fig. 10 Tensile properties: (a) Young's modulus and tensile strength and (b) strain at break of PVDF-based CLFO nanocomposite films.

nanoparticles. This attainment of relatively steady tensile strength can be ascribed to the uniform dispersion of nanoparticles with a moderate interfacial adhesion with the PVDF matrix, which is in direct agreement with the morphological observations of nanocomposite films. As part of this, the introduction of PVP and its compatibility with PVDF[80] enabled solid contacts to be established and helped increase the efficiency of interfacial stress transfer between nanoparticles and the PVDF matrix.[18] However, beyond this concentration, the tensile strength decreases, likely due to the same agglomeration issues affecting Young's modulus.[80]

The strain at break, an indicator of ductility and flexibility, also showed a significant improvement with the addition of CLFO nanoparticles. At 3 wt% CLFO, the strain at break increased by 33%, indicating enhanced flexibility and toughness of the nanocomposite films. This improvement can be ascribed to the effective dispersion of nanoparticles, which helps distribute stress more evenly across the matrix, thus allowing the material to deform more before breaking.[21] However, similar to Young's modulus and tensile strength, the strain at break decreases beyond 3 wt% CLFO. This reduction is likely due to the initial stages of nanoparticle clustering at higher concentrations, which creates stress concentration points and reduces the overall ductility and flexibility of the films.[80]

These results show that adding 3 wt% CLFO nanoparticles to the PVDF and PVP matrix is the optimal combination for

improving the mechanical properties, notably stiffness, strength, and ductility.

5. Conclusion

This study represents a meaningful step evolving in the development of piezoelectric materials for sustainable energy conversion. The synthesis of CLFO nanoparticles through co-precipitation and heat treatment has resulted in nanocomposite films with noticeably improved properties. The key findings reveal a significant increase in crystallinity, attributed to the nanoparticles acting as heterogeneous nucleating agents that facilitate PVDF crystallization. The electroactive β-phase content within the nanocomposite films reached 80%, which is crucial for harnessing the piezoelectric properties. Thermogravimetric analysis highlighted enhanced thermal stability imparted by the nanoparticles, making the films more resilient under varying temperature conditions. Mechanically, the addition of 3 wt% CLFO nanoparticles led to a 33% increase in the strain at break besides a 25% rise in Young's modulus. These advancements in structural, thermal, and mechanical properties, along with the significant presence of the polar β-phase, make the 3 wt% CLFO concentration in PVDF/PVP nanocomposite films optimal for both mechanical strength and piezoelectric efficiency. These findings make the *X*CLFO/PVP/PVDF nanocomposite films promising candidates for energy harvesting and other applications requiring efficient conversion of mechanical stress into electrical energy. The addition of CLFO nanoparticles enhances the piezoelectric properties, thereby also enhancing the dielectric properties of the PVDF matrix, making the films suitable for energy harvesting and sensing applications. The improved dispersion facilitated by PVP further contributes to the material's mechanical flexibility and functional performance, which are essential for applications like flexible sensors, wearable electronics, and biomedical devices. These enhancements enable the nanocomposites to efficiently convert mechanical energy into electrical signals or provide responsive sensing capabilities, which are a valuable addition to the field of piezoelectric materials and pave the way for future innovations in sustainable energy technology.

Data availability

The data that support the findings of this study are available from the corresponding author, Fatima-Zahra Semlali, upon reasonable request.

Conflicts of interest

There are no conflicts to declare.

Acknowledgements

We would like to thank the Moroccan Ministry of Higher Education, Scientific Research and Innovation and the OCP Foundation who funded this work through the APRD research program.

References

1 Z. He, *3D nanofibrous macrostructures for piezoelectric energy harvesting via electrospinning: electrospray of polyvinylidene fluoride based material*, HAL Id: tel-04105070, 2023.
2 S. Mishra, L. Unnikrishnan, S. K. Nayak and S. Mohanty, Advances in Piezoelectric Polymer Composites for Energy Harvesting Applications: A Systematic Review, *Macromol. Mater. Eng.*, 2019, **304**(1), 1–25.
3 B. Gusarov, *PVDF piezoelectric polymers: characterization and application to thermal energy harvesting*, 2015.
4 M. Boutaldat, N. Chakhchaoui, A. Eddiai, M. Meddad, O. Cherkaoui, M. Rguiti, *et al.*, Modeling and electromechanical performance analysis of polyvinylidene difluoride/textile-system for energy harvesting from the human body toward a novel class of self-powered sensors, *Polym. Adv. Technol.*, 2022, (May), 4–6.
5 F. Z. Semlali, A. Ait Benhamou, K. El Bourakadi, A. E. K. Qaiss, R. Bouhfid, J. Jacquemin, *et al.*, Thermo-compression process-mediated in-situ cellulose microfibers phosphorylation enables high performant cellulosic paper packaging, *Chem. Eng. J.*, 2023, **473**(March), 145268.
6 R. Farhan, A. Eddiai, M. Meddad, N. Chakhchaoui, M. Rguiti and M. Mazroui, Improvement in energy conversion of electrostrictive composite materials by new approach via piezoelectric effect: Modeling and experiments, *Polym. Adv. Technol.*, 2021, **32**(1), 123–130.
7 G. Kalimuldina, N. Turdakyn, I. Abay, A. Medeubayev, A. Nurpeissova, D. Adair, *et al.*, A review of piezoelectric pvdf film by electrospinning and its applications, *Sensors*, 2020, **20**(18), 1–42.
8 S. Waqar, L. Wang and S. John, Piezoelectric energy harvesting from intelligent textiles, *Electronic Textiles: Smart Fabrics and Wearable Technology*, Elsevier Ltd, 2015, pp. 173–197, DOI: **10.1016/B978-0-08-100201-8.00010-2**.
9 H. Kawai, Piezoelectricity Poly (vinylidene Fluoride), *Jpn. J. Appl. Phys.*, 1969, **8**(7), 975, DOI: **10.1143/JJAP.8.975**.
10 A. Mayeen and N. Kalarikkal, Piezoelectric Polymer Nanocomposites For Energy Scavenging Applications, *Polym. Nanostruct. Mater.*, 2019, 273–292.
11 Y. Cho, J. Jeong, M. Choi, G. Baek, S. Park, H. Choi, *et al.*, BaTiO3@PVDF-TrFE nanocomposites with efficient orientation prepared via phase separation nano-coating method for piezoelectric performance improvement and application to 3D-PENG, *Chem. Eng. J.*, 2022, **427**(March 2021), 131030, DOI: **10.1016/j.cej.2021.131030**.
12 K. Maity, S. K. Ghosh, M. Xie, C. R. Bowen and D. Mandal, Design of flexible piezoelectric-pyroelectric nanogenerator for self-powered wearable sensor, *AIP Conf. Proc.*, 2019, **2115**, 030604.
13 M. Khalifa, A. Mahendran and S. Anandhan, Durable, efficient, and flexible piezoelectric nanogenerator from electrospun PANi/HNT/PVDF blend nanocomposite, *Polym. Compos.*, 2019, **40**(4), 1663–1675.
14 A. Veved, G. W. Ejuh and N. Djongyang, Study of the chemical softness, chemical hardness, chemical stability

and interaction energy of the piezoelectric composite: (-CH2-CF2-)3/nHfO2, *Polym. Bull.*, 2021, **78**(9), 4977–4986, DOI: 10.1007/s00289-020-03346-6.

15 A. Veved, G. W. Ejuh and N. Djongyang, Review of emerging materials for PVDF-based energy harvesting, *Energy Rep.*, 2022, **8**, 12853–12870, DOI: 10.1016/j.egyr.2022.09.076.

16 E. M. Alharbi and A. Rajeh, Processing polymer film nanocomposites of poly(vinylidene fluoride)/poly(ethylene oxide) and cobalt oxide nanoparticles for flexible energy storage systems, *Opt. Quantum Electron.*, 2024, **56**(7), 1–25, DOI: 10.1007/s11082-024-07134-8.

17 P. Martins, C. M. Costa, G. Botelho, S. Lanceros-Mendez, J. M. Barandiaran and J. Gutierrez, Dielectric and magnetic properties of ferrite/poly(vinylidene fluoride) nanocomposites, *Mater. Chem. Phys.*, 2012, **131**(3), 698–705, DOI: 10.1016/j.matchemphys.2011.10.037.

18 J. Diani and K. Gall, Finite Strain 3D Thermoviscoelastic Constitutive Model, *Society*, 2006, 1–10.

19 J. Chang, M. Dommer, C. Chang and L. Lin, *Nano Energy*, 2012, **1**, 356–371, DOI: 10.1016/j.nanoen.2012.02.003.

20 M. Choi, G. Murillo, S. Hwang, J. W. Kim, J. H. Jung, C. Y. Chen, *et al.*, Mechanical and electrical characterization of PVDF-ZnO hybrid structure for application to nanogenerator, *Nano Energy*, 2017, **33**(December 2016), 462–468, DOI: 10.1016/j.nanoen.2017.01.062.

21 M. El Achaby, F. Z. Arrakhiz, S. Vaudreuil, E. M. Essassi and A. Qaiss, Piezoelectric β-polymorph formation and properties enhancement in graphene oxide - PVDF nanocomposite films, *Appl. Surf. Sci.*, 2012, **258**(19), 7668–7677, DOI: 10.1016/j.apsusc.2012.04.118.

22 H. Alhussain, A. M. Alghamdi, N. Y. Elamin and A. Rajeh, Recent Progress in Enhanced Optical, Mechanical, Thermal Properties, and Antibacterial Activity of the Chitosan/Polyvinylalcohol/Co3O4 Nanocomposites for Optoelectronics and Biological Applications, *J. Polym. Environ.*, 2024, **32**, 3735–3748, DOI: 10.1007/s10924-024-03191-y.

23 N. Y. Elamin, A. Modwi, W. Abd El-Fattah and A. Rajeh, Synthesis and structural of Fe3O4 magnetic nanoparticles and its effect on the structural optical, and magnetic properties of novel Poly(methyl methacrylate)/Polyaniline composite for electromagnetic and optical applications, *Opt. Mater.*, 2023, **135**(December 2022), 113323, DOI: 10.1016/j.optmat.2022.113323.

24 C. Wei, Z. Feng, M. Baisariyev, L. Yu, L. Zeng, T. Wu, *et al.*, Valence Change Ability and Geometrical Occupation of Substitution Cations Determine the Pseudocapacitance of Spinel Ferrite XFe2O4(X = Mn, Co, Ni, Fe), *Chem. Mater.*, 2016, **28**(12), 4129–4133.

25 L. Ourry, S. Marchesini, M. Bibani, S. Mercone, S. Ammar and F. Mammeri, Influence of nanoparticle size and concentration on the electroactive phase content of PVDF in PVDF-CoFe2O4-based hybrid films, *Phys. Status Solidi A*, 2015, **212**(2), 252–258.

26 M. Hashim, M. Raghasudha, S. S. Meena, J. Shah, S. E. Shirsath, S. Kumar, *et al.*, Influence of rare earth ion doping (Ce and Dy) on electrical and magnetic properties of cobalt ferrites, *J. Magn. Magn. Mater.*, 2018, **449**, 319–327, DOI: 10.1016/j.jmmm.2017.10.023.

27 P. D. Prasad and J. Hemalatha, Enhanced dielectric and ferroelectric properties of cobalt ferrite (CoFe2O4) fiber embedded polyvinylidene fluoride (PVDF) multiferroic composite films, *Mater. Res. Express*, 2019, **6**(9), 094007.

28 M. M. El-Masry and R. Ramadan, The effect of CoFe2O4, CuFe2O4 and Cu/CoFe2O4 nanoparticles on the optical properties and piezoelectric response of the PVDF polymer, *Appl. Phys. A: Mater. Sci. Process.*, 2022, **128**(2), 1–13, DOI: 10.1007/s00339-021-05238-6.

29 P. Biswas, N. A. Hoque, P. Thakur, M. M. Saikh, S. Roy, F. Khatun, *et al.*, Portable Self-Powered Piezoelectric Nanogenerator and Self-Charging Photo-Power Pack Using in Situ Formed Multifunctional Calcium Phosphate Nanorod-Doped PVDF Films, *Langmuir*, 2019, **35**(52), 17016–17026.

30 D. P. Pabba, B. V. B. Rao, A. Thiam, M. P. Kumar, R. V. Mangalaraja, R. Udayabhaskar, *et al.*, Flexible magnetoelectric PVDF–CoFe2O4 fiber films for self-powered energy harvesters, *Ceram. Int.*, 2023, **49**(19), 31096–31105, DOI: 10.1016/j.ceramint.2023.07.054.

31 A. Gebrekrstos, T. S. Muzata and S. S. Ray, Nanoparticle-Enhanced β-Phase Formation in Electroactive PVDF Composites: A Review of Systems for Applications in Energy Harvesting, EMI Shielding, and Membrane Technology, *ACS Appl. Nano Mater.*, 2022, **5**(6), 7632–7651.

32 H. Rekik, Z. Ghallabi, I. Royaud, M. Arous, G. Seytre, G. Boiteux, *et al.*, Dielectric relaxation behaviour in semi-crystalline polyvinylidene fluoride (PVDF)/TiO2 nanocomposites, *Composites, Part B*, 2013, **45**(1), 1199–1206, DOI: 10.1016/j.compositesb.2012.08.002.

33 J. Lee, J. Oba, N. Ohba and S. Kajita, Creation of crystal structure reproducing X-ray diffraction pattern without using database, *npj Comput. Mater.*, 2023, **9**(1), 135, DOI: 10.1038/s41524-023-01096-3.

34 J. Zhou, M. Wang, X. Shu, J. Ma, H. Ren, Y. Wang, *et al.*, Facile synthesis of La-doped cobalt ferrite@glucose-based carbon composite as effective multiband microwave absorber, *J. Am. Ceram. Soc.*, 2021, **104**(5), 2191–2200.

35 I. H. Gul and A. Maqsood, Structural, magnetic and electrical properties of cobalt ferrites prepared by the sol-gel route, *J. Alloys Compd.*, 2008, **465**(1–2), 227–231.

36 R. S. Yadav, I. Kuřitka, J. Vilcakova, J. Havlica, L. Kalina, P. Urbánek, *et al.*, Sonochemical synthesis of Gd3+ doped CoFe2O4 spinel ferrite nanoparticles and its physical properties, *Ultrason. Sonochem.*, 2018, **40**(August 2017), 773–783.

37 R. Kumar, R. K. Singh, M. K. Zope and M. Kar, Tuning of magnetic property by lattice strain in lead substituted cobalt ferrite, *Mater. Sci. Eng., B*, 2017, **220**, 73–81, DOI: 10.1016/j.mseb.2017.03.012.

38 L. Zhang, R. He and H. C. Gu, Oleic acid coating on the monodisperse magnetite nanoparticles, *Appl. Surf. Sci.*, 2006, **253**(5), 2611–2617.

39 S. R. Naik and A. V. Salker, Change in the magnetostructural properties of rare earth doped cobalt ferrites relative to the magnetic anisotropy, *J. Mater. Chem.*, 2012, **22**(6), 2740–2750.

40 N. Sanpo, C. C. Berndt and J. Wang, Microstructural and antibacterial properties of zinc-substituted cobalt ferrite nanopowders synthesized by sol-gel methods, *J. Appl. Phys.*, 2012, **112**(8), 084333, DOI: **10.1063/1.4761987**.

41 K. Mohit, V. R. Gupta, N. Gupta and S. K. Rout, Structural and microwave characterization of Ni0.2Co xZn0.8-xFe2O4 for antenna applications, *Ceram. Int.*, 2014, **40**(1 PART B), 1575–1586, DOI: **10.1016/j.ceramint.2013.07.045**.

42 M. H. Abdellatif, A. A. Azab and M. Salerno, Effect of rare earth doping on the vibrational spectra of spinel Mn-Cr ferrite, *Mater. Res. Bull.*, 2018, **97**(September 2017), 260–264, DOI: **10.1016/j.materresbull.2017.09.012**.

43 W. M. Prest and D. J. Luca, The formation of the γ phase from the α and β polymorphs of polyvinylidene fluoride, *J. Appl. Phys.*, 1978, **49**(10), 5042–5047.

44 S. Ez-Zahraoui, F. Z. Semlali Aouragh Hassani, R. Bouhfid, A. E. K. Qaiss and M. El Achaby, Strengthening effect of phosphate sludge by-product and styrene-butadiene rubber on the properties of high-density polyethylene composites, *Composites, Part A*, 2023, **166**(August 2022), 107378, DOI: **10.1016/j.compositesa.2022.107378**.

45 M. B. Mohamed, A. M. El-naggar, Z. K. Heiba and A. M. Kamal, Modifications in the structural, optical, and dielectric properties of PVA/PVP/PEG blend by incorporation of PANi/ZnWO4 nanohybrid for optoelectronic and energy storage devices, *Opt. Mater.*, 2024, **149**, 1221–1231.

46 P. Martins, C. M. Costa, M. Benelmekki, G. Botelho and S. Lanceros-Mendez, On the origin of the electroactive poly(vinylidene fluoride) β-phase nucleation by ferrite nanoparticles via surface electrostatic interactions, *CrystEngComm*, 2012, **14**(8), 2807–2811.

47 S. Labihi, N. Chakhchaoui, A. Eddiai, M. El Achaby, M. Meddad, O. Cherkaoui, *et al.*, Enhancement of piezoelectric β-polymorph formation and properties of graphene oxide and PZT-incorporated in PVDF-HFP matrix for energy harvesting applications, *Polym. Compos.*, 2023, **44**(4), 2296–2304.

48 Y. Kou, W. Zhou, X. Li, Z. Wang, Y. Li, H. Cai, *et al.*, Enhanced dielectric properties of PVDF nanocomposites with modified sandwich-like GO@PVP hybrids, *Polym.-Plast. Technol. Mater.*, 2020, **59**(6), 592–605.

49 D. Chipara, V. Kuncser, K. Lozano, M. Alcoutlabi, E. Ibrahim and M. Chipara, Spectroscopic investigations on PVDF-Fe2O3 nanocomposites, *J. Appl. Polym. Sci.*, 2020, **137**(30), 1–13.

50 T. T. Van Tran, S. R. Kumar, C. H. Nguyen, J. W. Lee, H. A. Tsai, C. H. Hsieh, *et al.*, High-permeability graphene oxide and poly(vinyl pyrrolidone) blended poly(vinylidene fluoride) membranes: Roles of additives and their cumulative effects, *J. Membr. Sci.*, 2021, **619**, 118773, DOI: **10.1016/j.memsci.2020.118773**.

51 S. Ez-Zahraoui, S. Sabir, S. Berchane, R. Bouhfid, A. E. K. Qaiss, F. Z. Semlali Aouragh Hassani, *et al.*, Toughening effect of thermoplastic polyurethane elastomer on the properties of fly ash-reinforced polypropylene-based composites, *Polym. Compos.*, 2022, (August), 1–12.

52 C. Behera, N. Pradhan, P. R. Das and R. N. P. Choudhary, Development of self-standing, lightweight and flexible polymer-cobalt ferrite nanocomposites for field sensor, *J. Polym. Res.*, 2022, **29**(2), 65, DOI: **10.1007/s10965-022-02916-8**.

53 M. S. Sebastian, A. Larrea, R. Gonçalves, T. Alejo, J. L. Vilas, V. Sebastian, *et al.*, Understanding nucleation of the electroactive β-phase of poly(vinylidene fluoride) by nanostructures, *RSC Adv.*, 2016, **6**(114), 113007–113015.

54 P. Martins, C. Caparros, R. Gonçalves, P. M. Martins, M. Benelmekki, G. Botelho, *et al.*, Role of nanoparticle surface charge on the nucleation of the electroactive β-poly(vinylidene fluoride) nanocomposites for sensor and actuator applications, *J. Phys. Chem. C*, 2012, **116**(29), 15790–15794.

55 K. Cai, X. Han, Y. Zhao, R. Zong, F. Zeng and D. Guo, A Green Route to a Low Cost Anisotropic MoS2/Poly(Vinylidene Fluoride) Nanocomposite with Ultrahigh Electroactive Phase and Improved Electrical and Mechanical Properties, *ACS Sustain. Chem. Eng.*, 2018, **6**(4), 5043–5052.

56 H. Gunti, *Structural, spectral and dielectric properties of PVDF-HFP/cobalt ferrite composite films*, 2023, pp. 1–20.

57 S. Rostom, W. B. Tyler, G. Yuan, T. Saito and M. D. Dadmun, Polymer chain diffusion in all-polymer nanocomposites: Confinement vs chain acceleration, *J. Phys. Chem. C*, 2020, **124**(34), 18834–18839.

58 S. Supriya, L. Kumar and M. Kar, Optimization of dielectric properties of PVDF–CFO nanocomposites, *Polym. Compos.*, 2019, **40**(3), 1239–1250.

59 G. Suresh, S. Jatav, M. S. Ramachandra Rao and D. K. Satapathy, Enhancement of dielectric and ferroelectric properties in cobalt ferrite doped poly(vinylidene fluoride) multiferroic composites, *Mater. Res. Express*, 2017, **4**(7), 075301, DOI: **10.1088/2053-1591/aa7109**.

60 A. Bhiogade, K. Nagamalleswari, P. Mandal and V. K. M. Ramakrishnan, Flexible multiferroic PVDF/CoFe2O4 composite films for pyroelectric energy conversion, *J. Mater. Sci.*, 2023, **58**(47), 17805–17815, DOI: **10.1007/s10853-023-09149-0**.

61 H. L. He, Z. B. Pan, X. J. Lv, Z. C. Li, M. K. Wang, J. H. Zhao, *et al.*, Modulated magnetostriction and multiferroic properties in the PVDF-based cobalt ferrite particulate composites, *Mater. Chem. Phys.*, 2024, **325**, 129780, DOI: **10.1016/j.matchemphys.2024.129780**.

62 M. Koç, Ç. E. D. Dönmez, L. Paralı, A. Sarı and S. Aktürk, Piezoelectric and magnetoelectric evaluations on PVDF/CoFe2O4based flexible nanogenerators for energy harvesting applications, *J. Mater. Sci.: Mater. Electron.*, 2022, **33**(10), 8048–8064.

63 R. Gonçalves, P. M. Martins, C. Caparrós, P. Martins, M. Benelmekki, G. Botelho, *et al.*, Nucleation of the electroactive β-phase, dielectric and magnetic response of poly(vinylidene fluoride) composites with Fe2O 3 nanoparticles, *J. Non-Cryst. Solids*, 2013, **361**(1), 93–99, DOI: **10.1016/j.jnoncrysol.2012.11.003**.

64 A. Pal and I. M. S. Gaur, *Investigation of structural and thermal characteristics of PVDF/ZnO nanocomposites*, 2013, pp. 821–830.

65 M. F. Uddin and C. T. Sun, Improved dispersion and mechanical properties of hybrid nanocomposites, *Compos. Sci. Technol.*, 2010, **70**(2), 223–230, DOI: **10.1016/j.compscitech.2009.09.017**.

66 F. Beygmohammdi, H. Nourizadeh Kazerouni, Y. Jafarzadeh, H. Hazrati and R. Yegani, Preparation and characterization of PVDF/PVP-GO membranes to be used in MBR system, *Chem. Eng. Res. Des.*, 2020, **154**(December), 232–240, DOI: **10.1016/j.cherd.2019.12.016**.

67 N. V. Lakshmi, P. Tambe and N. K. Sahu, Giant permittivity of three phase polymer nanocomposites obtained by modifying hybrid nanofillers with polyvinylpyrrolidone, *Compos. Interfaces*, 2018, **6440**, DOI: **10.1080/09276440.2017.1338876**.

68 M. A. Tofighy, High-flux PVDF/PVP nanocomposite ultrafiltration membrane incorporated with graphene oxide nanoribbones with improved antifouling properties, *J. Appl. Polym. Sci.*, 2021, **138**(4), 49718, DOI: **10.1002/app.49718**.

69 H. Mahdavi, N. Mazinani and A. A. Heidari, Poly(vinylidene fluoride) (PVDF)/PVDF-g-polyvinylpyrrolidone (PVP)/TiO2 mixed matrix nanofiltration membranes: preparation and characterization, *Polym. Int.*, 2020, **69**(12), 1187–1195.

70 C. U. Gradišar, M. Mihelčič, V. Bobnar, M. Remškar and L. Slemenik Perše, The Effect of PVP on Thermal, Mechanical, and Dielectric Properties in PVDF-HFP/PVP Thin Film, *Coatings*, 2022, **12**(9), 1241, DOI: **10.3390/coatings12091241**.

71 H. M. Ragab, Improved Physical, thermal, and conductivity strength of ternary nanocomposite films of PVDF/PMMA/GO NPs for electrical applications, *J. Polym. Res.*, 2022, **29**(6), 219, DOI: **10.1007/s10965-022-03060-z**.

72 B. J. Cha, Effect of High-Temperature Spinning and PVP Additive on the Properties of PVDF Hollow Fiber Membranes for Microfiltration, *Macromol. Res.*, 2006, **14**(6), 596–602.

73 A. Islam, A. N. Khan and M. F. Shakir, Strengthening of β polymorph in PVDF/FLG and PVDF/GO nanocomposites, *Mater. Res. Express*, 2020, **7**, 015017, DOI: **10.1088/2053-1591/ab5f82**.

74 T. Lin, Y. Li, J. Wang and J. You, Effect of pmma molecular weight on its localization during crystallization of pvdf in their blends, *Polymers*, 2021, **13**(23), 1–12.

75 F. Semlali Aouragh Hassani, M. El Achaby, M. O. Bensalah, D. Rodrigue, R. Bouhfid and A. Qaiss, Injection molding of short fiber thermoplastic bio-composites: Prediction of the fiber orientation, *J. Compos. Mater.*, 2020, **54**(30), 1–11.

76 F. Z. Semlali Aouragh Hassani, W. Ouarhim, M. El Achaby, Y. Tamraoui, M. O. Bensalah, D. Rodrigue, *et al.*, Recycled tires shreds based polyurethane binder: Production and characterization, *Mech. Mater.*, 2020, **144**, 1–10.

77 Y. Zare, Assumption of interphase properties in classical Christensen-Lo model for Young's modulus of polymer nanocomposites reinforced with spherical nanoparticles, *RSC Adv.*, 2015, **5**(116), 95532–95538, DOI: **10.1039/C5RA19330C**.

78 A. Schneider, G. Francius, R. Obeid, P. Schwinté, J. Hemmerlé, B. Frisch, *et al.*, Polyelectrolyte multilayers with a tunable young's modulus: Influence of film stiffness on cell adhesion, *Langmuir*, 2006, **22**(3), 1193–1200.

79 I. Erukhimovich and M. O. de la Cruz, *Phase equilibria and charge fractionation in polydisperse polyelectrolyte solutions*, 2004, pp. 1466–1473, **https://arxiv.org/abs/cond-mat/0406218**, DOI: **10.1002/polb**.

80 Z. Guo, X. Xu, Y. Xiang, S. Lu and S. P. Jiang, New anhydrous proton exchange membranes for high-temperature fuel cells based on PVDF-PVP blended polymers, *J. Mater. Chem. A*, 2015, **3**(1), 148–155.